Cement and Concrete Composites 141 (2023) 105124

Contents lists available at ScienceDirect

Cement and Concrete Composites

journal homepage: www.elsevier.com/locate/cemconcomp

Enhancement of surface properties of cementitious materials by phosphate treatments

Hélène Pasco [a], Sonia Naidu [b], Barbara Lothenbach [c], Enrico Sassoni [a,*]

[a] Dept. of Civil, Chemical, Environmental & Materials Engineering (DICAM), University of Bologna, Bologna, Italy
[b] Dept. of Construction Products, Saint-Gobain Research Paris, Aubervilliers, France
[c] Concrete & Asphalt Laboratory, Empa, Dübendorf, Switzerland

ARTICLE INFO

Keywords:
Portland cement
Diammonium hydrogen phosphate
Potassium hydrogen phosphate
Hydroxyapatite
Calcium phosphates
Thermodynamic modeling

ABSTRACT

This study aims at investigating the ability of aqueous phosphate solutions to improve the surface properties of cement pastes *via* the formation of low-solubility calcium phosphate (CaP) phases. Diammonium hydrogen phosphate (DAP), dipotassium hydrogen phosphate (DPP) and disodium hydrogen phosphate (DSP) were investigated based on thermodynamic modeling and experiments. For DPP, the influence of concentration and cement age was evaluated. A 1 M DPP + 1 mM $CaCl_2$ solution applied to cement hydrated for 7 days was most promising. The CaP coating formed after 24 h of exposure resulted in significant improvements in the cement pastes' resistance to abrasion, surface indentation and staining. Preliminary durability tests by immersion in water were successfully carried out to ascertain that no efflorescence due to soluble salts appeared and that mechanical improvement was retained. Compared to DAP, DPP has the advantage of not releasing NH_3 into the atmosphere, thus preventing unpleasant odor and improving the treatment's environmental sustainability.

1. Introduction

Since its discovery in the 19th century, the use of Portland cement has continuously increased, and is today the most widely used material in the world after water [1]. Both in new and existing buildings, including in cultural heritage, the enhancement of the surface properties of cementitious mortars, plasters and concrete is extremely important. In new buildings, improvements in hardness, abrasion resistance and stain resistance are desired to increase the durability of floors, renders and façades, thus reducing the need for maintenance. In existing buildings, numerous deterioration processes, such as freeze-thaw cycles, salt crystallization and corrosion of reinforcement steel bars induced by carbonation and chloride ingress, may lead to cracking, scaling or pulverization of cementitious materials [2–4], for which consolidation is required.

To improve the surface properties of concrete and cementitious substrates, several strategies can be adopted. According to the classification provided by the European Standard 1504-2 (2004) [2], treatments for the surface protection of concrete can be distinguished by: (i) "*hydrophobic impregnation*" (typically by silanes or siloxanes, this treatment produces a water-repellent surface, while pores and capillaries are internally coated, but not filled); (ii) "*impregnation*" (typically by organic polymers, this treatment reduces the surface porosity and strengthens the surface, by partially or totally filling the pores and capillaries); or (iii) "*coating*" (typically by organic polymers, possibly with addition of cement as a filler, this treatment produces a continuous protective layer on the concrete surface).

Among the readily available solutions [5,6], organic treatments often exhibit limitations due to their poor compatibility with the cementitious substrate, low durability when exposed in the field, release of VOCs and poor fire resistance [7–9]. Therefore, a lot of research in the last decade has focused on inorganic solutions that can enhance durability. Amongst them, ethyl silicate has provided encouraging results [10–12], although the hydrophobicity it induces is temporary [8].

In the present study, we investigated a new strategy for surface enhancement of cementitious materials, based on *in situ* formation of low-solubility inorganic calcium phosphate coatings (CaP) on the substrate. This strategy was inspired by research carried out in the last decade on the conservation of carbonate-based substrates, such as marble, limestone and lime-based mortars [13–15]. The principle is to form CaP phases *in situ via* a wet precipitation reaction between calcium ions available from the substrate and phosphate ions supplied by the addition of an aqueous phosphate precursor, such as diammonium hydrogen phosphate (DAP). As the dissolution of the substrate may be

* Corresponding author.
E-mail address: enrico.sassoni2@unibo.it (E. Sassoni).

https://doi.org/10.1016/j.cemconcomp.2023.105124
Received 6 January 2023; Received in revised form 14 April 2023; Accepted 5 May 2023
Available online 6 May 2023
0958-9465/© 2023 The Authors. Published by Elsevier Ltd. This is an open access article under the CC BY license (http://creativecommons.org/licenses/by/4.0/).

the rate-limiting step, calcium ions may also be supplied directly with the phosphate solution, by adding a soluble calcium source such as $CaCl_2$. This has been demonstrated to significantly favor formation of CaP films on marble [14].

These CaP phases typically include hydroxyapatite (HAP, $Ca_{10}(PO_4)_6(OH)_2$), carbonated HAP ($Ca_{10-x}(PO_4)_{6-x}(CO_3)_x(OH)_{2-x-2y}(CO_3)_y$) [16] and octacalcium phosphate (OCP, $Ca_8H_2(PO_4)_6{\cdot}5H_2O$) [15]. Due to the very low water solubility products of these phases (K_{sp} 10^{-117} for HAP, 10^{-97} for OCP [17] compared to 10^{-9} for $CaCO_3$ [18] at 25 °C), their presence was found to reduce the dissolution of the carbonate substrates in acidic rain [19,20]. As the aqueous DAP solution is also able to penetrate the substrate in depth (for porous or cracked substrates, up to more than 1 cm from the surface [21]), the formation of new CaP phases at grain boundaries also significantly improved bulk mechanical properties of weathered limestone, marble and lime-based mortars [15].

Based on the promising results obtained on natural stones and lime-based mortars, a more recent study in the field of conservation of heritage buildings investigated the ability of reaction with DAP solutions to improve the mechanical properties of mortars based on natural hydraulic lime (NHL) and Portland Cement (CEM I 32.5 R) [22]. Significant increases in dynamic elastic modulus and compressive strength were obtained (the magnitude depending on the concentration of DAP), without dramatically altering the pore structure or water absorption ability of the underlying substrate [22].

In addition to the synthesis of CaP *via* wet precipitation, an alternative biogenic route has also been investigated for *in situ* formation of HAP [23,24]. By treating cementitious substrates with suitable bacteria and a growth medium, HAP can be formed as a metabolic product of the bacteria, with a positive outcome on substrate properties (e.g. diminished surface roughness and hydrophobic behavior) [23,24]. However, this route is significantly more complex compared to the wet precipitation route to enable widespread application.

The present study aims at 1) investigating the potential to form low solubility calcium phosphate coatings on cementitious substrates *via* wet precipitation of aqueous phosphates, 2) assessing the improvement they can confer on the durability of the cementitious substrates and 3) maximizing the performance of said coatings *via* the optimization of the various reaction parameters. For simplicity's sake, tests were carried out on cement pastes, in the view of extending the results to mortars and concrete in the future. The rationale of the study can be summarized as follows.

1) *Selection of the aqueous phosphate precursor*. We screened three different precursors, namely diammonium hydrogen phosphate (DAP, $(NH_4)_2HPO_4$), dipotassium hydrogen phosphate (DPP, K_2HPO_4) and disodium hydrogen phosphate (DSP, Na_2HPO_4), with the goal of choosing the most promising one for moving forward. Only ammonium phosphate had been tested on natural stones [15], as it was then reasoned that potassium and sodium phosphates could have introduced soluble salts which may be detrimental for stone conservation. However, with cementitious materials, small amounts of sodium and potassium are already present in the substrate. Also, as DPP and DSP have never been investigated, we do not know whether they are indeed detrimental for durability. Furthermore, compared to DAP, both DPP and DSP have the advantage of not releasing NH_3 into the atmosphere, which, although not dangerous in the quantities released, has a strong odor and can be an irritant to an applicator in indoor environments. Therefore, DPP and DSP were also investigated. The effects of the three aqueous precursors were evaluated in terms of phases formed (XRD and SEM-EDS) and performance conferred (*via* resistance to abrasion, indentation and staining). Laboratory experiments were coupled with thermodynamic modeling to obtain further insight into the expected CaP phases. Finally, the stability of the new CaP phases, the possible formation of efflorescence after immersion in water and the possible release of soluble phosphates into water were investigated and, for the selected precursor, it was ascertained that the beneficial effects were retained after immersion in water.
2) *Selection of precursor concentration*. For the most promising precursor, various concentrations were tested, to identify maximum performance enhancement possible with the minimum amount of precursor required. The optimal concentration was selected based on results of mechanical tests, i.e. resistance to abrasion, staining and indentation, again complemented with phase characterization (XRD and SEM-EDS) and thermodynamic modeling.
3) *Selection of cement age when exposed to treatment*. For the selected precursor and concentration, the influence of cement curing time (1, 7 or 28 days) was evaluated using the same techniques detailed above, with the aim of identifying the best time to apply the phosphate treatment to maximize improvements obtained.
4) *Thermodynamic modeling*. Thermodynamic modeling was used to predict the phases formed when hydrated cement is reacted with each of the three precursors and at the various concentrations, as a complement to the experimental study. In this way, the experimental conditions that may lead to any high-solubility CaP phases or other undesirable phases may be excluded.

2. Materials and methods

2.1. Thermodynamic modeling

The GEMS software [25] was used to predict the most thermodynamically stable phases to form from the reactions between hardened Portland cement and the various aqueous phosphate precursors. This software minimizes the Gibbs free energy of the entire system to reach thermodynamic equilibrium and predicts which phases should form as a function of the reaction parameters (e.g. pH or precursor concentration). In addition to the general PSI-Nagra database [26], the Cemdata18 database [27] was used to describe hydrated Portland cement together with thermodynamic data on magnesium and calcium phosphates [28–32] to predict the thermodynamically stable outcome of reacting aqueous phosphate solutions with cement. The formation of quartz, Al-containing siliceous hydrogarnet and magnesite was suppressed due to kinetic reasons.

To account for ammonium containing solids, data for struvite ($MgNH_4PO_4{\cdot}6H_2O$), dittmarite ($MgNH_4PO_4{\cdot}H_2O$), NH_4-taranakite ($(NH_4)_3Al_5(HPO_4)_6(PO_4)_2{\cdot}18H_2O$), basic ammonium aluminate phosphate ($NH_4Al_2(PO_4)_2OH{\cdot}2H_2O$), $(NH_4)_2AlH(PO_4)_2{\cdot}4H_2O$ and of $NH_4AlPO_4OH{\cdot}2H_2O$ were added as summarized in Table 1.

In the presence of aluminium, also Al-containing phosphates might form such as taranakite or OH-minyulite [31]. At pH values below 3, NH_4-taranakite ($(NH_4)_3Al_5(HPO_4)_6(PO_4)_2{\cdot}18H_2O$) is expected to form, while between pH 3 to 5 the minyulite-like basic ammonium aluminate phosphate ($NH_4Al_2(PO_4)_2OH{\cdot}2H_2O$) has been observed to form [54,55]. Recalculations based on the experimental data reported in Taylor and Gurney [54,55] and considering the formation of Al-phosphate complexes as detailed in Xu et al. [31] resulted in solubility products of $10^{-188.5}$ for NH_4-taranakite and of $10^{-47.3}$ for the minyulite-like phase, as compiled in Table 1. The derived solubility products of NH_4-taranakite and of $NH_4AlPO_4OH{\cdot}2H_2O$ are comparable to the solubility products derived for the K-containing analogues [31]. At pH values above 6, $(NH_4)_2AlH(PO_4)_2{\cdot}4H_2O$ is formed, while at lightly basic conditions $NH_4AlPO_4OH{\cdot}2H_2O$ could form, although the formation of struvite or ammonium calcium phosphate hydrate might be favoured under most conditions [56]. The measured concentration in Taylor et al. [56] were used to derive a solubility product of $10^{-54.1}$ for $(NH_4)_2AlH(PO_4)_2{\cdot}4H_2O$ and of $10^{-19.5}$ for $NH_4AlPO_4OH{\cdot}2H_2O$ (see Table 1).

No measured solubility data were available for potassium or ammonium calcium phosphate hydrate, $KCaPO_4{\cdot}H_2O$ or $NH_4CaPO_4{\cdot}H_2O$. The solubility of $KCaPO_4{\cdot}H_2O$ was roughly estimated from the solubility $MgKPO_4{\cdot}H_2O$ (see Table 1) and the observations of the

Table 1
Solubility products (log K^{o}_{so}) of ammonium phosphate containing solids at 25 °C and 1 bar added to the Cemdata18 and thermodynamic data on magnesium and calcium phosphates.

Solids	Reaction	Volume (cm^3/mol)	log $K_{so}°$ (kJ/mol)	$\Delta_f G°$	Reference[a]
Struvite	$MgNH_4PO_4{\cdot}6H_2O \Leftrightarrow Mg^{2+} + NH_4^+ + PO_4^{3-} + 6H_2O$	144.3[b]	−13.4	−3051.61	ts
Dittmarite	$MgNH_4PO_4{\cdot}H_2O \Leftrightarrow Mg^{2+} + NH_4^+ + PO_4^{3-} + H_2O$	71.0[c]	−13.2	−1864.6	ts
NH_4-Taranakite	$(NH_4)_3Al_5(HPO_4)_6(PO_4)_2{\cdot}18H_2O \Leftrightarrow 3NH_4^+ + 6H^+ + 5\ Al^{3+} + 8PO_4^{3-} + 18H_2O$	629.4[d]	−188.5	−16151.2	ts
Basic ammonium aluminate phosphate	$NH_4Al_2(PO_4)_2OH{\cdot}2H_2O + H^+ \Leftrightarrow NH_4^+ + 2\ Al^{3+} + 2PO_4^{3-} + 3H_2O$	128.7[e]	−47.3	−4065.6	ts
	$(NH_4)_2AlH(PO_4)_2\ 4H_2O \Leftrightarrow 2NH_4^+ + Al^{3+} + H^+ + 2PO_4^{3-} + 4H_2O$	162.1[f]	−54.1	−3937.1	ts
	$NH_4AlPO_4OH\ 2H_2O + H^+ \Leftrightarrow NH_4^+ + Al^{3+} + PO_4^{3-} + 3H_2O$	81.9[g]	−19.5	2404.8	ts
Nanocrystalline hydroxyapatite *tentative value*	$Ca_5(PO_4)_3(OH)_{am} \Leftrightarrow 5Ca^{2+} + 3PO_4^{3-} + OH^-$	159.6	−55.0[h]	−6291.1	ts [30,33],
Potassium calcium phosphate hydrate *tentative value*	$KCaPO_4{\cdot}H_2O \Leftrightarrow K^+ + Ca^{2+} + PO_4^{3-} + H_2O$	69.4[i]	−12.9[j]	−2164.8	ts
Ammonium calcium phosphate hydrate *tentative value*	$NH_4CaPO_4{\cdot}H_2O \Leftrightarrow NH_4^+ + Ca^{2+} + PO_4^{3-} + H_2O$	71.2[k]	−13.6[l]	−1965.8	ts

[a] Ts: this study.
[b] Volume calculated from XRD data: density 1.70 g/cm^3. [34]. S = 369 J/mol/K; C_p 353 J/mol/K, both calculated from K-struvite [28], $(NH_4)_2SO_4$ and K_2SO_4 [35] assuming $\Delta S_r = \Delta C_{p,r.} = 0$ following the procedure outlined by [36].
[c] Volume calculated from XRD data: density 2.19 g/cm^3. [37,38]. S = 164 J/mol/K; C_p = 153 J/mol/K, both calculated from struvite and structural water [37] assuming $\Delta S_r = \Delta C_{p,r.} = 0$.
[d] Volume calculated from XRD data: density 2.03 g/cm^3. [39].
[e] Volume calculated from XRD data: density 2.45 g/cm^3. [40].
[f] No structural data available, volume estimated from newberyite, dittmarite, berlinite farringtonite and structural water; density 2.01 g/cm^3.
[g] No structural data available, volume estimated from basic ammonium aluminate phosphate and berlinite ($AlPO_4$); density 2.36 g/cm^3.
[h] Hydroxyapatite solubility reported in [30] increased by 3 log units following the observations of [33] for nanocrystalline hydroxyapatite.
[i] Volume calculated from XRD data: density 2.77 g/cm^3. [41].
[j] Solubility estimated from $MgKPO_4$ H_2O, whitelockite ($Ca_3(PO_4)_2$) and farringtonite ($Mg_3(PO_4)_2$) [28].
[k] Volume estimated from $KCaPO_4{\cdot}H_2O$, K-struvite [28] and struvite; l solubility calculated from the concentration measurements reported in [42]. Where available, the solubility of the different phosphate containing hydrates was recalculated based on published measured equilibrium concentrations, following the procedure outlined e.g. in Lothenbach et al. [28]. In particular, for struvite ($MgNH_4PO_4{\cdot}6H_2O$) and dittmarite ($MgNH_4PO_4{\cdot}H_2O$) several studies have reported equilibrium concentrations under different conditions, which allowed to derive their solubility from 5 to 85 °C as detailed in Fig. 1. The solubility of struvite varies only very moderately with temperature, while the solubility of the dewatered dittmarite clearly decreases (Fig. 1), comparable to the solubility behavior of the structural analogue K-struvite and its dewatered form, $MgKPO_4{\cdot}H_2O$ [28]. The stabilisation of dittmarite at increased temperature agrees also well with experimental observation reported in literature [43,44].

formation of $CaKPO_4{\cdot}H_2O$ at pH values above 14 reported by Xu et al. [57]. The solubility of $NH_4CaPO_4{\cdot}H_2O$ was estimated from the concentrations reported in Fordham & Schürmann [42]. In the calculations the formation of nanocrystalline (or poorly crystalline) hydroxyapatite was considered, instead of crystalline hydroxyapatite, with a 3 log units higher solubility based on Moreno et al. [33] as the formation of crystalline hydroxyapatite is kinetically very slow. In the thermodynamic calculations, the formation of crystalline hydroxyapatite is supressed due to kinetic reasons, in agreement with the experimental observations in the present study.

For the modeling, the XRF composition of the Portland cement used in the experimental tests was used as detailed in Table 2, assuming complete reaction of the cement. The gradual changes towards the surface of the cement exposed to the different phosphate solutions are simulated by increasing the amount of exposure solution. This allows to mimic the changes observed experimentally towards the surface of cement, mortar or concrete specimens as detailed e.g. in Lothenbach et al. [58]. Such simplified thermodynamic models are very flexible and allow easy parameter variations and the results are in many cases comparable to full transport modeling, where parameters such as porosity and tortuosity have to be known in detail.

Table 2
Elemental analyses of the Portland cement used in this study.

Oxide	Quantity (wt%)
CaO	62.9
SiO_2	19.3
Al_2O_3	4.80
Fe_2O_3	3.36
MgO	3.66
SO_3	4.40
K_2O	0.94
Na_2O	0.43
P_2O_5	0.12
Cr_2O_3	0.02
MnO	0.05
SrO	0.14
TiO_2	0.27
ZnO	0.04
CO_2 (TGA)	0.53
LOI 105–950 °C	1.11
LOI 20–105 °C	0.60

2.2. Sample preparation

Portland Cement (PC, CEM I 52.5 R, Italcementi) was used as substrate. Its elemental composition is reported in Table 2. X-Ray fluorescence (XRF; PANalytical X MagixPro PW2540) was used to quantify oxides, sulphur analyzer (Horiba EMIA 920V2) to quantify SO_3, TGA to quantify the CO_2 content and loss on ignition (LOI) to evaluate the total content of hydrates and carbonates. Phase composition of the PC was determined using X-ray diffraction (XRD; Bruker D8 Advance) with quantification by Rietveld refinement (Table 3).

Cement pastes were prepared in a Hobart mixer, using deionized water with a water-to-binder ratio of 0.4. Slabs with 16 × 14 × 2 cm^3 size were prepared in steel molds. After curing for the first 24 h at 20 ±

Table 3
Phase composition of the PC used in this study quantified by Rietveld refinement.

Phases	Quantity (%)
C_3S	57.5
C_2S	10.1
C_4AF	9.8
C_3A	3.2
MgO	3.4
Gypsum	1.4
$Ca(OH)_2$	0.5
Anorthite	1.1
Arcanite	1.1
Non-identified	11.8

1 °C and 90% RH, the slabs were demolded and further cured in the same conditions until the nominal curing time was reached (1, 7 or 28 days). The slabs were next cut into 7 × 7 × 2 cm^3 prisms using a wet saw and then dried in an oven at 40 °C until constant mass to stop cement hydration.

2.3. Sample treatment

The treatments consisted in immersing already hardened cement pastes into aqueous solutions containing the various phosphate precursors. Diammonium hydrogen phosphate (DAP, $(NH_4)_2HPO_4$, Supelco), dipotassium hydrogen phosphate (DPP, K_2HPO_4, Sigma Aldrich) and disodium hydrogen phosphate (DSP, Na_2HPO_4, Bioreagent) were used as phosphate sources. Calcium chloride ($CaCl_2$, Acros Organics) was added to the solutions to favor faster formation of CaP films, as previously demonstrated on marble [14]. For the lowest precursor concentration tested (0.1 M DPP), ethanol was added to the solution as it had been shown on marble to favor formation of a dense CaP coating [59,60]. The formulations adopted for the various steps of the study are summarized in Table 4.

The concentration of the DAP formulation (1 M DAP + 1 mM $CaCl_2$) was selected based on previous studies on natural stone [14,15], which highlighted its high effectiveness in forming new calcium phosphates with protective and consolidating action, without leaving undesired soluble phosphates in the substrate. The concentration of the DPP formulation was selected to mimic that of DAP, while for DSP (for which a 1 M concentration could not be reached) a concentration close to saturation was used (0.4 M DSP + 0.4 mM $CaCl_2$).

The prismatic specimens were immersed in the respective solutions in plastic containers, adopting a 3:1 solution:cement ratio (i.e. 300 mL of solution per 100 g of cement paste). Initially, the specimens were saturated by capillarity (with the surface to be analyzed facing down, suspended on a plastic grid) and then totally submerged with the solution after the wet front had reached the upper face of the specimens. They were left to react in the sealed containers for 24 h at room temperature, as measured from the point of initial solution introduction.

Table 4
Phosphate-based formulations tested in the study.

Goal	Treatment formulation	Cement age
Precursor selection (DAP, DPP or DSP)	1 M DAP + 1 mM $CaCl_2$ 1 M DPP + 1 mM $CaCl_2$ 0.4 M DSP + 0.4 mM $CaCl_2$	XRD and SEM-EDS: 28 d Abrasion, indentation and stain: 7 d
Optimal concentration selection (2 M, 1 M or 0.1 M)	0.1 M DPP + 0.1 mM $CaCl_2$ + 30%v EtOH 1 M DPP + 1 mM $CaCl_2$ 2 M DPP + 2 mM $CaCl_2$	XRD and SEM-EDS: 28 d Abrasion, indentation and stain: 7 d
Selection of cement age at treatment (1, 7 or 28 d)	1 M DPP + 1 mM $CaCl_2$	XRD and SEM-EDS: 1, 7, 28 d Abrasion, indentation and stain: 1, 7, 28 d

Reference untreated samples (labeled as "UT") were prepared by submerging them in DI water for the same amount of time at the same temperature. At the end of the treatment, the samples were removed from solution and rinsed in DI water for 15 min (to remove any remaining unreacted phosphate precursor) and then dried in an oven at 40 °C until constant mass (about 48 h, to prevent further cement hydration).

For XRD and SEM-EDS analyses, the phosphate treatments were performed on powders to facilitate phase identification. After curing for 28 days, untreated slabs were crushed into small pieces with a maximum diameter of 1 mm. Cement hydration was arrested by solvent exchange in isopropanol [61], followed by drying at 40 °C for 24 h. The powders were then immersed in phosphate solutions at a 3:1 solution:cement ratio. At the end of the treatment, the powders were rinsed with water and dried again by solvent exchange followed by oven drying at 40 °C for 24 h.

2.4. Sample characterization

Mineralogical composition. X-Ray Diffraction (XRD) was performed on hardened cement powders (obtained by crushing hardened cement pastes) after treatment with the phosphate solutions. XRD was performed on powders (rather than massive samples) to have a higher quantity of CaP with respect to the cementitious substrate and hence stronger XRD peaks owing to the new CaP. A Malvern PANalytical Empyrean X-ray diffractometer was used (Cu tube with K_α radiation λ = 1.5405 Å, 40 kV and 30 mA, 2θ range = 4–45°, step size = 0.013°, time per step = 178 s).

Morphology and chemical composition. Morphological assessment was conducted *via* scanning electron microscopy equipped with a field emission gun (FEG-SEM, Tescan Mira3, WD = 10 mm, voltage = 10 kV), on graphite sputter-coated powders. Elemental composition was determined by energy dispersive spectroscopy (EDS, Bruker probe) on the whole area imaged by SEM (unless otherwise specified).

Abrasion resistance. The resistance to abrasion was measured on untreated and treated slabs, following a protocol developed for stones [62]. The weight loss per area (mg/cm^2) was determined after 50 min of a rotatory motion (300 rpm) of steel balls and corundum powder against the sample surface. Three replicates were tested for each condition.

Surface hardness. Surface indentation was performed to assess the surface hardness of untreated and treated paste slabs, using a durometer (Zwick-Roell, digital Shore D hardness tester, 50 N). At least ten measurements, distributed across the specimen surface, were taken for each treatment condition.

Stain resistance. 0.1 mL of black coffee was applied on the surface of treated and reference untreated paste slabs and left for 1 min, before being rinsed off with DI water (3 mL) and paper. Colorimetric differences (La*b* coordinates) were measured before staining and after stain removal attempt and drying for 24 h, using a NH310 colorimeter. The before vs. after color differences ΔE^* were assessed according to the formula $\Delta E^* = (\Delta L^{*2} + \Delta a^{*2} + \Delta b^{*2})^{1/2}$. The lower the ΔE^*, the lower the residual staining from coffee and hence the higher the stain resistance of a coated sample. For each condition, two measurements were performed on three replicate samples, for a total of 6 measurements per condition.

Efflorescence risk and treatment durability. Efflorescence risk was determined by immersing treated slabs in DI water for 12 h. Water was allowed to saturate the samples *via* capillarity, with the treated surface facing up to facilitate transport of soluble fractions to the surface. Then, the samples were rinsed with tap water and dried in an oven for 24 h. Finally, the surfaces were visually inspected for any efflorescence formation. Separately, preliminary evaluation of treatment durability was conducted by immersing treated cement powders in water for 24 h, with the water being renewed every 2 h for the first 10 h, and then repeating SEM-EDS analyses to check for any phase transformations or loss. Subsequent analyses were conducted for the selected precursor, whereby 3

treated slabs were immersed in DI water and dried as described in section 2.1, then tested to assess resistance to abrasion, indentation and staining, so as to determine if any decrease in the beneficial effects of the treatment occurred post-water immersion.

Ion chromatography. The possible leaching of phosphate ions when samples are exposed to water was assessed by ion chromatography on phosphate-treated and untreated samples, for comparison's sake. The phosphate treatments were applied on hydrated paste samples, cured for 28 days, following the procedure described in section 2.1. For ion chromatography, 1 g of hydrated powder that had been exposed to the phosphate treatments was immersed in 100 mL of DI water and extraction was performed by leaving the samples in a shaking incubator ICF 400PLUS for 1 h at 30 °C. The obtained solution was filtered and 1 mL of the filtrate was analyzed by ion chromatography (Dionex ICS1000) equipped with an IonPac AS14A analytical column (4 × 250 mm) combined with an ASRS-Ultra conductivity suppressor. The eluent was a solution of 8 mM Na_2CO_3 and 1 mM $NaHCO_3$ in DI water, and the flow rate was 1.1 mL/min.

Water uptake. The effect of the treatments on the pore system of the cement pastes was evaluated by the capillary water absorption test, performed on untreated and treated samples following the European Standard 15801 (2010) for porous inorganic materials [63]. The slabs were placed on a wet bedding layer made of sheets of filter paper soaked with DI water in a flat and closed plastic container. The mass increase over time (0, 5, 10, 20, 30, 45, 90 min and 24 h) was plotted versus the square root of time. The water absorption coefficient (AC, $g/(cm^{-2}{\cdot}s^{-1/2})$) was determined according to the method described in [63], i.e. as the slope of the linear section of the curve (in our case, constituted of 5 points between 10 and 45 min).

3. Results and discussion

3.1. Selection of the aqueous phosphate precursor

The expected changes at the surfaces of PC exposed to diammonium phosphate (DAP), dipotassium phosphate (DPP), or disodium phosphate (DSP) solutions were calculated using thermodynamic modeling to guide the selection of the treatment conditions to be investigated experimentally and are reported in Fig. 2. The volume of the phases present in 100 g of unhydrated Portland cement (y-axis) is given as a function of the volume of solution used to react 100 g of cement (x-axis). By exposing hydrated cement to increasing amounts of the various phosphate solutions, the amount of cement hydrates such as C–S–H, portlandite, ettringite, hydrotalcite and siliceous hydrogarnet progressively decrease and new phases are formed. In all three cases, the formation of (nanocrystalline) hydroxyapatite, HAP, is predicted near the surface. Other calcium phosphate (CaP) phases, such as brushite or octacalcium phosphate (OCP) are less stable and thus not predicted. This can be explained by the fact that (nanocrystalline) HAP is the most thermodynamically stable CaP phase in these conditions [64], and so metastable phases such as OCP are expected to eventually convert to HAP. Near the surface, the formation of potassium or ammonium calcium phosphate hydrate and of a minor amount of struvite (for DAP) is predicted. Other phosphate minerals (e.g. struvite, K-struvite and Na-struvite) are expected to form at high solution/sample ratios, which are less realistic in field conditions (i.e. tens of liters of solution would be needed to react 100 g of cement). Importantly, very soluble K- or Na-containing salts that may lead to efflorescence were not predicted. As such and to avoid the presence of those phases, a 3:1 solution/sample mass ratio was adopted in the subsequent experiments. This is indicated by the dotted lines in Fig. 2. As the three precursors did not show major differences in this region and did not lead to undesirable soluble phases, they were all adopted for the subsequent experiments.

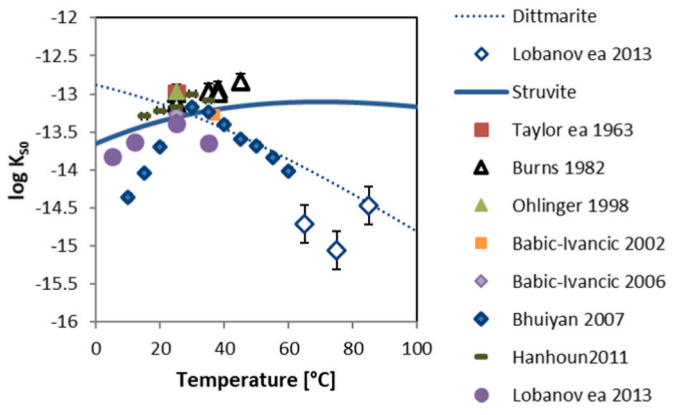

Fig. 1. Calculated solubility products for struvite ($MgNH_4PO_4{\cdot}6H_2O \Leftrightarrow Mg^{2+} + NH_4^+ + PO_4^{3-} + 6H_2O$) and dittmarite ($MgNH_4PO_4{\cdot}H_2O \Leftrightarrow Mg^{2+} + NH_4^+ + PO_4^{3-} + H_2O$) as a function of temperature based on the experimental data reported by [43,45–49] and the solubility constants derived in [50–53]. The solid line indicates the solubility of K-struvite calculated from the thermodynamic data compiled in Table 1; the dashed line indicates the calculated solubility product of dittmarite.

Cement powders treated with phosphate solutions at a 3:1 solution/sample mass ratio and analyzed by XRD revealed clear differences between the three treated samples and the untreated reference, as shown in Fig. 3. A broad peak at 2-theta angle 26° and a shoulder around 31.5–32° (marked with stars in Fig. 3) can be detected in the treated samples. These signals correspond to the main peaks of HAP (JCPDS 96-901-3628). The fact that HAP is revealed by small and broad peaks can be ascribed to the low amount and poor crystallinity of HAP formed after treatment, likely nanocrystalline in nature. Formation of OCP (its strongest peak being at 4.7°) can be excluded, as no XRD peaks were present at this angle (Fig. 3). Traces of brushite (main peak at 11.6°) can be detected in the sample treated with DAP.

The formation of new CaP phases was further confirmed by SEM-EDS, as shown in Fig. 4. After treatment with DAP, new crystals with flower-like morphology, typical for HAP [14], were observed. Neither OCP nor brushite, which tend to have typical morphologies (flakes and platelets, respectively [14]), were observed (Fig. 4). EDS conducted on the crystals formed after DAP-treatment revealed the presence of calcium, phosphorous and oxygen elements, in addition to carbon coming from graphite sputtering, while no nitrogen or other elemental signals were detected. This rules out the likelihood of these crystals being due to any residual unreacted DAP or struvite, which would contain nitrogen, as well as cementitious hydrates. Compared to DAP, DPP and DSP treatments resulted in finer coatings (Fig. 4), composed of smaller needle-like crystals. No isolated crystals containing K or Na were revealed by SEM-EDS, which supports the thermodynamic modeling results that did not predict formation of K- or Na-containing salts or struvite phases (Fig. 2). Nonetheless, in addition to Ca, P and O, EDS analysis performed on the new CaP coatings revealed some potassium and sodium signals in the presence of the respective precursors.

The K and Na signals may be due to: (i) *adsorption* of K^+ and Na^+ ions onto the HAP surface; (ii) *incorporation* of these ions into the HAP crystals, thus producing K- and Na-substituted HAP [65] or (iii) the formation of some K- or Na-calcium phosphate hydrates intermixed with HAP. Depending on which mechanism is occurring, issues may arise when the treated cement is exposed to water: (i) in case of *adsorption*, the ions may be desorbed upon contact with water, and either be washed away (without leaving any undesired residue) or form efflorescence (thus leaving unaesthetic stains on the surface or potentially harmful compounds below the surface); (ii) in case of *incorporation*, the resulting substituted HAP may be more water soluble than stoichiometric HAP, so the beneficial effects of the treatment may be decreased upon exposure to water. In fact, in the case of sodium it has been pointed out in the biomedical literature that Na^+ ions in the surrounding aqueous solution are unfavorable to HAP formation [66] and their incorporation into the HAP crystal results in increased solubility [67,68]. The effect of K^+ ions

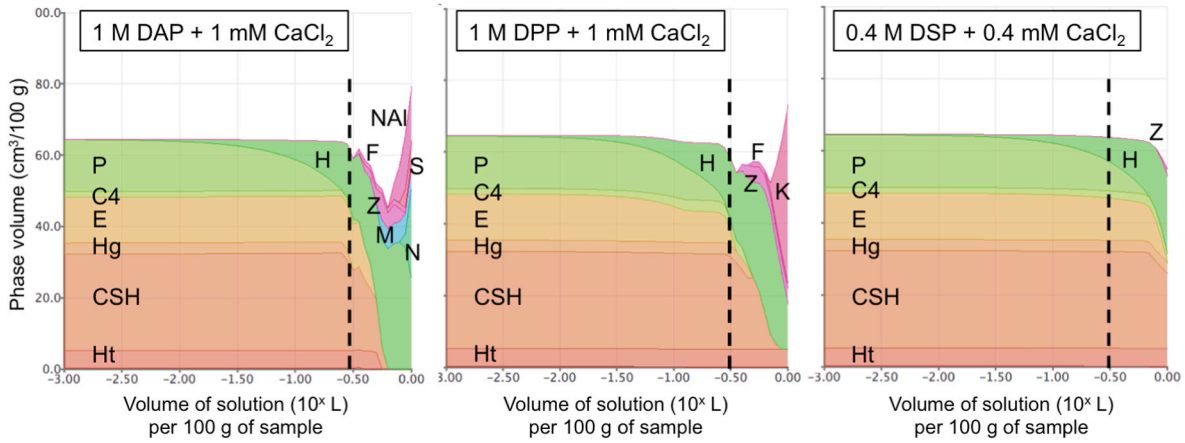

Fig. 2. Results of thermodynamic modeling (phase volume as a function of solution volume per 100 g of cement paste) for the three precursors. The dotted line indicates the solution/sample ratio adopted experimentally. P: Portlandite, C4: monocarbonate AFm (C_4AcH_{11}), E: Ettringite, Hg: siliceous hydrogarnet, Ht: Hydrotalcite, H: (nanocrystalline) hydroxyapatite, Z: Zeolite, M: Mg silicate hydrate, F: Ferrihydrite, S: amorphous siica, NAl: $(NH_4)_2AlH(PO_4)_2$, N: $Ca(NH_4)PO_4{\cdot}H_2O$, K: $CaK(PO_4){\cdot}H_2O$.

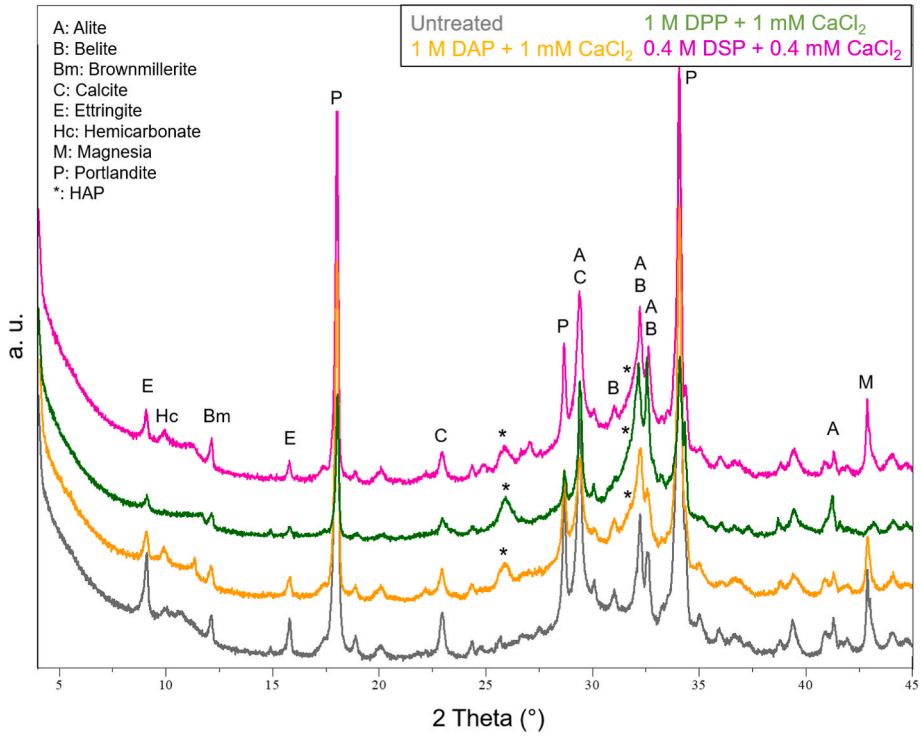

Fig. 3. XRD spectra of the untreated reference and samples treated with the three precursors.

has been studied less in the literature than Na^+ ions, but K^+ ions (138 pm radius) are much larger than Na^+ (102 pm radius) and Ca^{2+} ions (100 pm radius) [69], hence their incorporation into the HAP structure is less likely.

Overall, the coatings formed using DPP and DSP show promising features (fine crystals, absence of formation of soluble salts or struvite phases), but the presence of K and Na in the EDS spectra suggests the need to test the stability of the treated specimens when exposed to water, to check whether these ions are washed away with water or efflorescence is formed on the sample surface or the CaP coatings themselves dissolve in water.

When the samples treated with the three precursors were immersed in water for 12 h and then dried, in all cases the CaP coatings were still present after the test and showed clear Ca and P peaks when analyzed by EDS (Fig. 4). In the case of DAP, some difference in coating morphology was observed, while the coatings formed with the other precursors looked unaffected. With DPP, the potassium peak was no longer detected after water immersion, while for DSP the sodium peak was diminished. This suggests that these ions were apparently adsorbed onto the coatings and were washed away after water immersion. The possibility that K^+ and Na^+ ions were originally incorporated into the HAP crystal seems unlikely, because this would have led to increased water solubility of the CaP coatings, which on the contrary appear unaffected after water immersion. In none of the cases were isolated crystals observed *via* SEM-EDS or detected by XRD that could be ascribed to a K- or Na-containing salt. Nonetheless, to further exclude possible efflorescence formation, treated slabs were immersed in water for 12 h and the sample surfaces then visually inspected after drying. As shown in Fig. 5, no signs

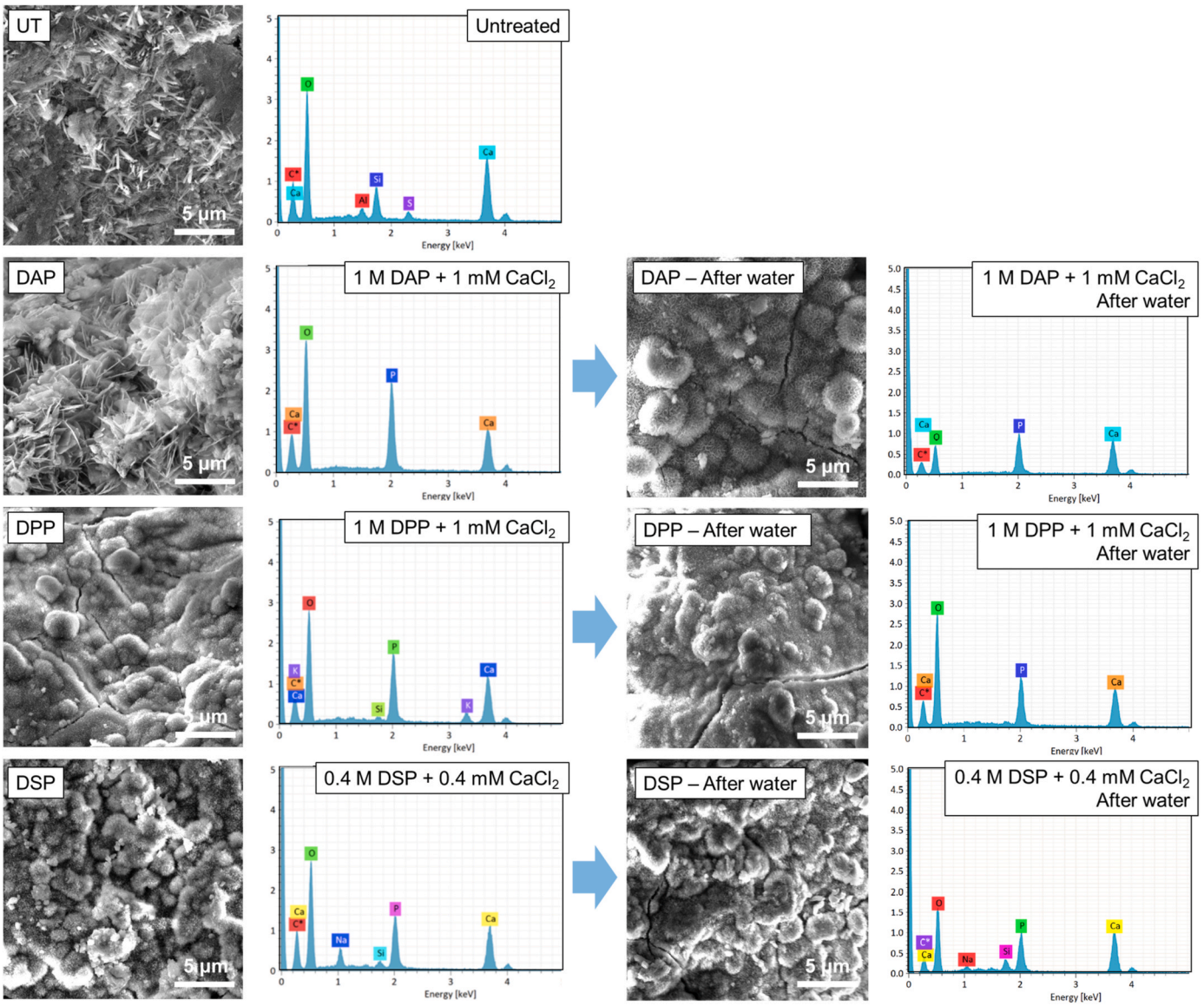

Fig. 4. SEM images and EDS spectra of the untreated reference and samples treated with the three precursors, before and after immersion in water to check their stability.

of efflorescence were detected on the sample surfaces, so the hypothesis that K^+ and Na^+ were originally adsorbed onto the HAP surface and then washed away by water seems confirmed.

It is noteworthy that, although no efflorescence was detected by any of the test performed, the release of some soluble phosphates into the water used for the immersion test may still have occurred. In practical applications, the release of soluble phosphates might have negative consequences for the environment. To ascertain whether soluble phosphates could be released after the immersion of treated samples in water, ion chromatography was carried out. As shown in Fig. 6 (left), for all the treatment conditions the amount of phosphate ions released in solution after 1 h at 30 °C was basically comparable to that released by the untreated cement (which initially contained 0.12 wt% of P_2O_5, Table 2). Therefore, in real applications, the risk of release of soluble phosphates from treated cementitious surfaces into the environment seems excluded.

The new CaP phases formed after treatment led to the improvements in surface properties illustrated in Fig. 7. In terms of abrasion resistance, the three precursors led to comparable decreases in material loss post-abrasion, with up to ~80% improvement. In the case of surface hardness, DPP and DAP resulted in the highest improvement, which reached ~5%. The fact that the improvement in abrasion resistance was much higher than that of resistance to surface indentation is likely due to the different depths from the external surface reached by the two techniques, as the depth reached by surface indentation is sensibly higher than that reached by abrasion. In terms of resistance to staining, DPP and DSP showed a remarkable capacity of allowing stain removal (the residual color change being below the visibility limit of $\Delta E^* = 2.3$ [70]), while in the case of DAP the residual stain was lower than for the untreated reference, but still visible. A possible reason for the better performance of DPP and DSP compared to DAP could be that the former precursors lead to apparently smoother coatings composed of finer crystals, while the flower-like morphology of the coating formed by DAP may result in higher roughness, which could make stain removal less easy. However, considering that, alongside surface roughness, several other parameters may influence the ease of stain removal (e.g. the substrate's initial color, open porosity and pore size distribution, wettability, drying rate), all these properties should be assessed to fully explain the observed behavior. In any case, it is noteworthy that, after immersion in water for 12 h to test treatment durability, the coffee stain

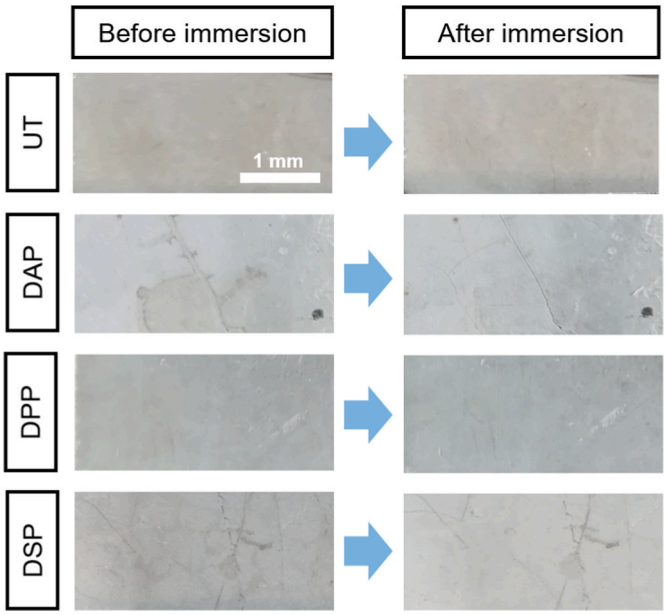

Fig. 5. Appearance of the surface of untreated and treated specimens before and after immersion in water for 12 h followed by drying.

also became invisible in the case of DAP, as shown in Fig. 5.

As both mechanical improvement and stain removal are influenced by the effects of the phosphate treatments on the pore system, the alterations in open porosity and pore size distribution were assessed by determining the variations in the water absorption coefficient (AC), measured by letting water penetrate the specimens through the treated surface. As shown in Fig. 6, the differences in AC between untreated and treated specimens appear as not significant, given the overlapping of the respective error bars. Therefore, it is possible to conclude that the phosphate treatments do not significantly alter the pore system of the substrate, which is in agreement with previous findings on stones and mortars [15].

Based on the results discussed above, all the phosphate treatments caused significant improvements in surface properties and exhibited sufficient stability. Considering its high effectiveness in improving abrasion resistance, surface hardness and stain removal (Fig. 7), as well as the lower likelihood of potassium incorporation into the HAP structure and the advantage of not releasing NH_3 gas into the atmosphere, DPP was selected as the most promising precursor for the continuation of the study. To further investigate whether prolonged contact with water could have negative effects on treatment performance, mechanical tests were carried out also on samples that had been immersed in water for 12 h. As shown in Fig. 8, only negligible decreases in the mechanical improvement and stain removal ability were registered (mostly within the error margin of measurements), thus further suggesting the stability of the new CaP phases.

3.2. Selection of precursor concentration

Thermodynamic modeling was performed to investigate the effects of using different concentrations of the DPP precursor on the nature and the amount of the new phases expected to form. As shown in Fig. 9, different DPP concentrations gave similar results in terms of composition of the new phases, with HAP and potassium calcium phosphate hydrate ($KCaPO_4{\cdot}H_2O$) being the main CaP phases formed. The main difference observed was in the solution/sample ratio required to obtain analogous compositions. For 2 M DPP, at the solution/sample ratio used experimentally (dashed line in Fig. 9), some $KCaPO_4{\cdot}H_2O$ and possibly zeolites (or zeolitic precursors) are predicted to form in addition to HAP. Compared to 1 M and 2 M DPP, the 0.1 M formulation required more

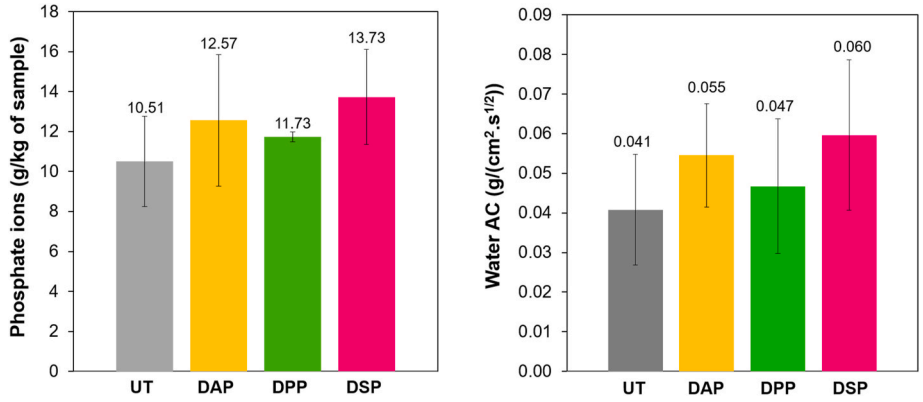

Fig. 6. Phosphate ions leached from untreated and treated cement powders (left) and water absorption coefficient (AC) of untreated and treated cement slabs (right).

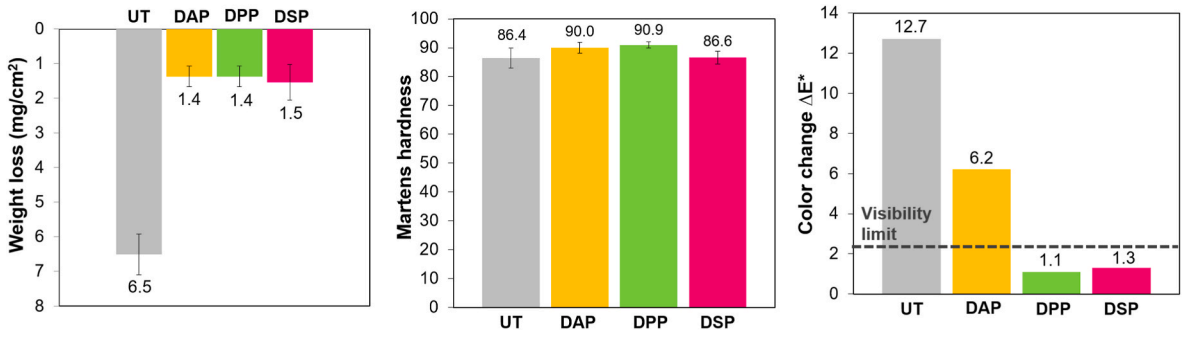

Fig. 7. Resistance to abrasion (left), indentation (center) and staining (right) of the untreated reference and samples treated with the three precursors.

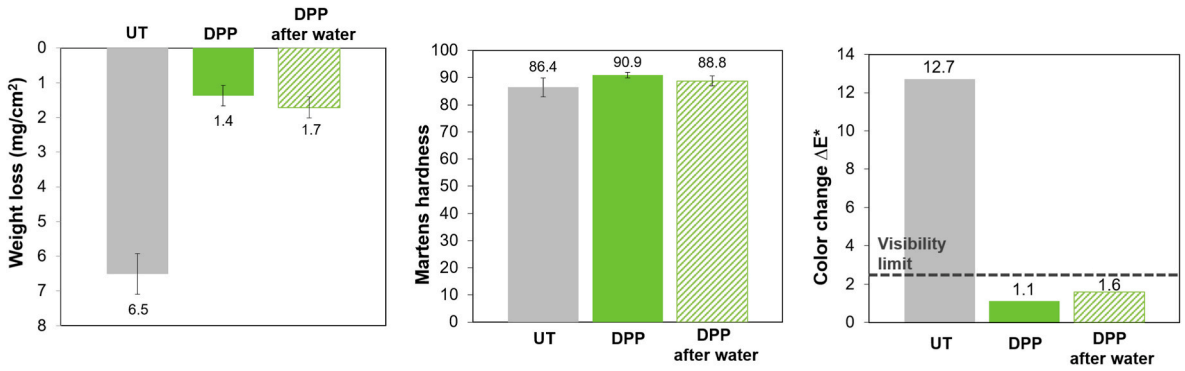

Fig. 8. Resistance to abrasion (left), indentation (center) and staining (right) after treatment with DPP, before (solid green bars) and after (dashed green bars) immersion in water for 12 h. (For interpretation of the references to color in this figure legend, the reader is referred to the Web version of this article.)

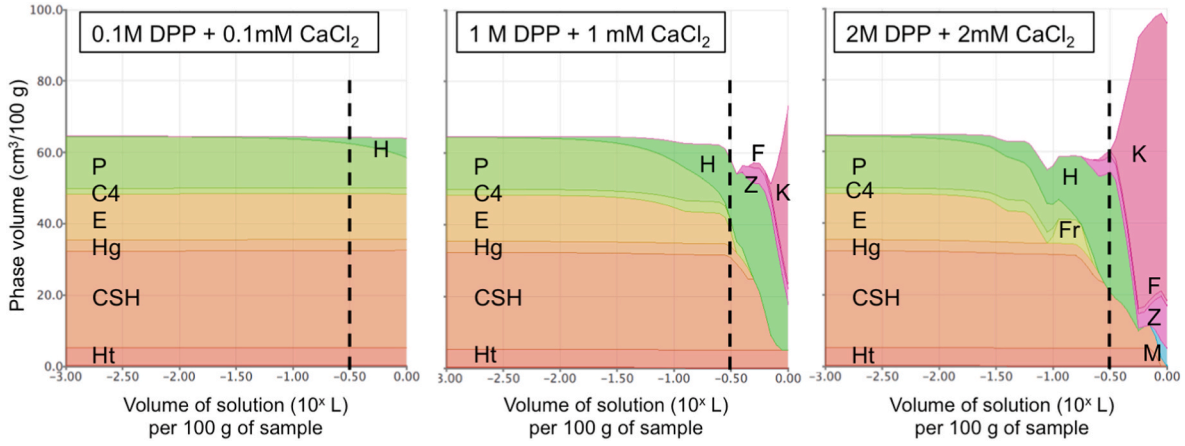

Fig. 9. Results of thermodynamic modeling (phase volume as a function of solution volume for 100 g of cement paste) for the three DPP concentrations. The dotted line indicates the solution/sample ratio adopted experimentally. P: Portlandite, C4: monocarbonate AFm (C_4AcH_{11}), E: Ettringite, Hg: siliceous hydrogarnet, Ht: Hydrotalcite, H: (nanocrystalline) hydroxyapatite, Z: Zeolite, M: Mg silicate hydrate, F: Ferrihydrite, Fr: Friedels salt + hemicarbonate, K: $CaKPO_4{\cdot}H_2O$.

solution to obtain the same phase distributions, so that, for the same solution/sample ratio selected in the previous step of the study (dashed line in Fig. 9), very low amounts of HAP were predicted. It is noteworthy that ethanol was added to the 0.1 M DPP +0.1 mM $CaCl_2$ solution to encourage the formation of homogenous coatings of CaP (as shown for DAP solutions in the case of natural stone [60]), which was neglected in the thermodynamic modeling due to lack of thermodynamic data describing the interaction of ethanol with phosphates.

The powders treated with the three concentrations of DPP solutions and analyzed by XRD revealed that, in the case of the 0.1 M DPP formulation, no clear evidence of HAP formation was obtained (Fig. 10), because of the low amount of HAP formed for the 0.1 M formulation, as predicted by thermodynamic modeling. In the case of the 1 M DPP formulation, a clear signal attributed to nanocrystalline HAP (marked by a star in Fig. 10) was detected, as described in the previous section. In the case of the 2 M DPP solution, HAP peaks were not observed, while clear peaks of potassium calcium phosphate hydrate ($KCaPO_4{\cdot}H_2O$) were detected in agreement with the thermodynamic modeling. Large crystals containing potassium, calcium, phosphorous and oxygen elements, therefore compatible with $KCaPO_4{\cdot}H_2O$, were found by SEM-EDS analysis, as detailed in the following.

SEM observation of the coatings showed that a similar morphology, composed of small needle-like crystals, was present in the three cases, the main difference being the formation of large, isolated crystals in the case of the 2 M DPP formulation (Fig. 11). EDS analysis detected Ca and P in all treated samples, as well as a K content increasing with the DPP concentration (K content of 0.8–1.9–3.5 atomic% for 0.1-1-2 M DPP). The large, isolated crystals observed in the 2 M DPP sample were found

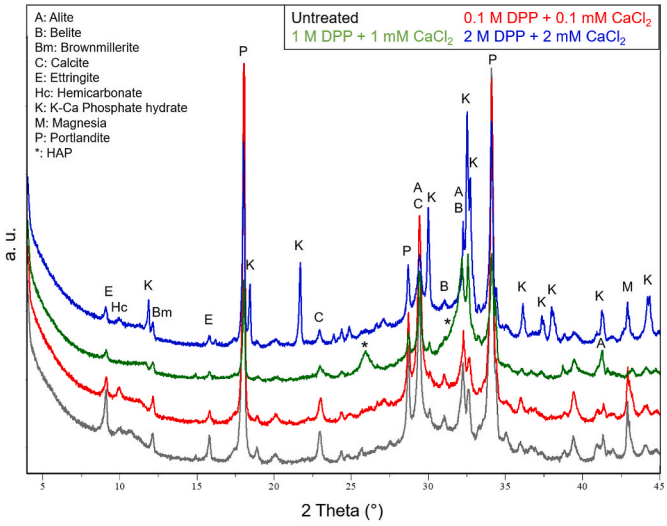

Fig. 10. XRD spectra of the untreated reference and samples treated with the 3 DPP formulations.

to contain Ca, P and a high K content (7.5 atomic%) and are thought to be $KCaPO_4{\cdot}H_2O$ crystals. In the EDS spectra of the 0.1 M and 2 M DPP samples, low signals of elements owing to the cementitious substrate (Si, Al, Mg, Na) were also detected, which suggests that the HAP coating

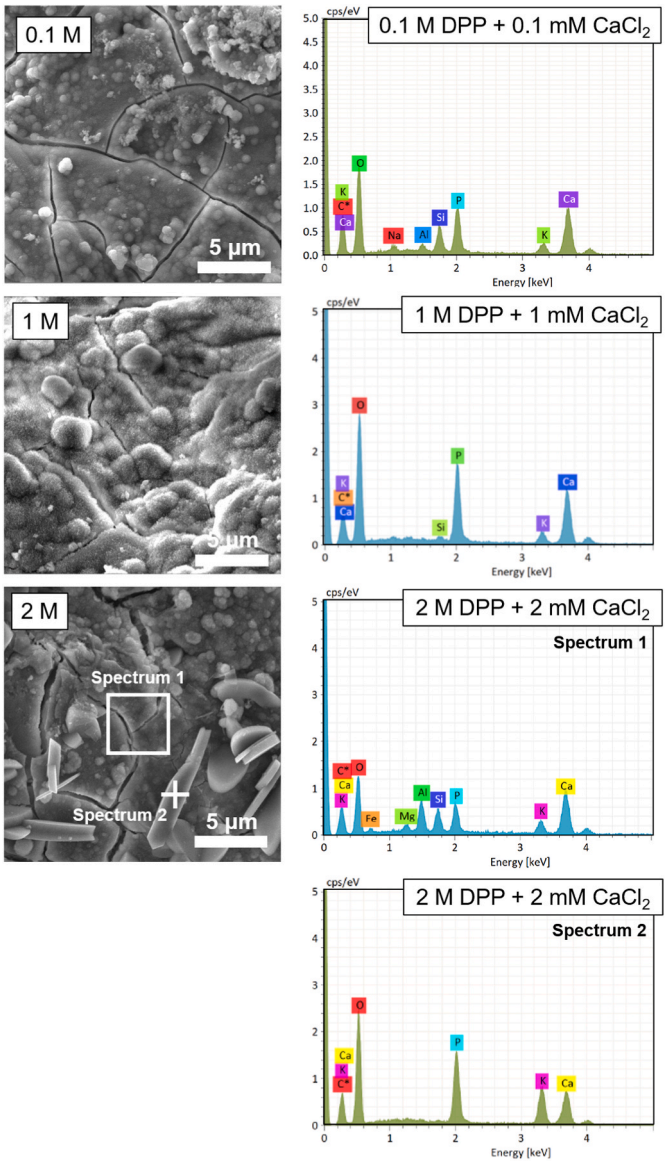

Fig. 11. SEM images and EDS spectra of samples treated with the three DPP formulations (for the 2 M DPP sample, the two EDS spectra were acquired in the two indicated areas, while for the other two samples EDS was performed on the whole imaged area).

may be thinner in these two cases, compared to the 1 M DPP coating. While in the case of the 0.1 M DPP formulation the lower thickness of the HAP coating can be easily ascribed to the lower precursor concentration, in the case of the 2 M DPP sample the low thickness could be originated by part of the phosphate ions being consumed to form the large $KCaPO_4{\cdot}H_2O$ crystals, instead of the HAP layer.

It is noteworthy that, independently of the concentration of the precursor, all the coatings exhibited cracks (Fig. 11), which may be a concern for the effectiveness and the durability of the treatment. Coatings are known to experience cracking during drying when they contain pores [71]. The tendency to crack decreases as the thickness of the coating is reduced and cracking is prevented when the coating thickness is below a critical level, because cracking becomes thermodynamically unfavorable [71]. In a previous study on CaP formation on stone using DAP as precursor, reducing the DAP concentration to 0.1 M and adding alcohol was found to be an effective strategy to densify the CaP coating and prevent cracking [60]. In the present study, also the sample treated with 0.1 M DPP and alcohol addition exhibited cracking. This may imply that the coating thickness is still above the critical level, but a possible contribution to cracking coming from sample preparation (*i.e.* high vacuum needed for SEM observation) should also be considered. To reduce cracking, possible strategies such as organic solvent addition [60] or nanoparticle addition [72] could be investigated in the future.

In terms of enhancement of the surface properties of the cementitious substrates, the abrasion resistance proved to progressively improve for increasing DPP concentration, although the benefit passing from 0.1 M to 1 M DPP was much higher than passing from 1 M to 2 M DPP (Fig. 12). The reason why the 2 M DPP formulation was not significantly more effective than the 1 M one could be that part of the phosphate ions was consumed to form $KCaPO_4{\cdot}H_2O$ crystals. These crystals appear to be deposited over the HAP coating, possibly without strong adhesion to the underlying coating. Both in terms of surface hardness and stain removal, no definite trend was present for increasing DPP concentration: the 1 M DPP formulation performed better than the 0.1 M one, likely because a thicker coating was formed, but the 2 M DPP formulation was less effective than the 1 M one. This could again be due to the formation of $KCaPO_4{\cdot}H_2O$ crystals over the CaP coating, thus reducing the surface hardness if they are not strongly bonded to the underlying coating and worsening the stain removal by increasing the surface roughness.

Considering that the 0.1 M DPP formulation led to smaller improvements in surface properties and that the 2 M DPP formulation resulted in large $KCaPO_4{\cdot}H_2O$ crystals, which potentially impacted surface hardness and stain removal and could also reduce the treatment durability, the intermediate 1 M DPP formulation was selected as the most promising solution to carry forward in the next section to identify the most favorable hydration age of the cement when the treatment may be applied.

3.3. Selection of cement age when exposed to treatment

Cement hydration age may be important in influencing the treatment efficacy and the final properties of the coating, due to differences in the substrate properties (e.g. pore size distribution and strength) at the time of phosphate introduction. These in turn could affect the thickness of the coating, film porosity and surface mechanical resistance.

As shown in Fig. 13, whether 1, 7 or 28 days of cement curing had occurred when the treatment was applied, the XRD spectra were similar, showing a broad peak and a shoulder at 2-theta angles of 26° and 31.5–32° respectively, compatible with the HAP signals. Some differences in the properties of the coatings formed at the different cement curing times were detected by SEM (Fig. 14), the coatings formed after 7 and 28 days covering the surface in a more continuous way than that formed after 1 day. This suggests that applying the phosphate treatment when the cement is older than 1 day could be advantageous.

In the untreated samples, both the abrasion resistance and the resistance to indentation showed a progressive increase for increasing curing time, the change between 7 and 28 days being more pronounced than between 1 and 7 days (Fig. 15). In the case of abrasion resistance, the phosphate treatment caused a similar improvement by 75–80% for any curing time (1, 7 or 28 days). In terms of resistance to indentation, samples cured for 1 and 7 days showed similar improvements after treatment by 4–5%, while a lower improvement after treatment (only 1%) was registered for the 28 days sample, which had higher initial hardness (Fig. 15). The fact that the improvement caused by HAP is higher when the initial surface hardness is lower is consistent with previous results obtained on natural stone, when the strengthening effect of HAP was found to be higher for more deteriorated stones [13], because the lower the cohesion of the substrate, the higher the bonding effect of HAP.

As for stain removal ability, the untreated references showed a clear trend, the residual stain becoming more and more visible as the curing time increased (Fig. 15). A possible reason could be that the progressive densification of the cement substrate over time, involving a reduction in open porosity and a reduction in the pore size [73], might make it more

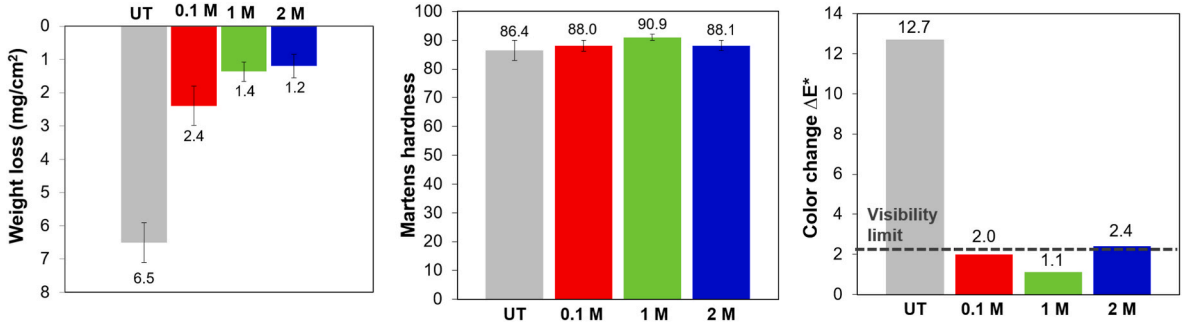

Fig. 12. Resistance to abrasion (left), indentation (center) and staining (right) of the untreated reference and samples treated with different DPP formulations.

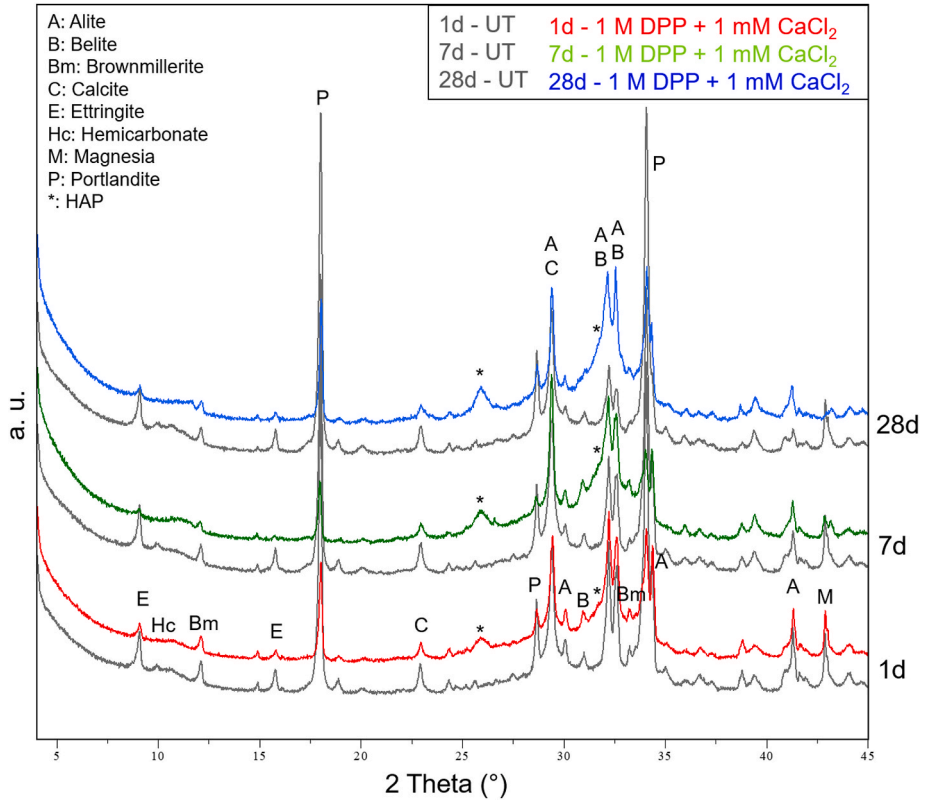

Fig. 13. XRD spectra of the untreated references and samples treated with DPP at different times.

difficult to remove the coffee stain from thinner pores, where coffee is absorbed more in depth. After treatment with the 1 M DPP solution, the stain removal ability was greatly increased, the improvement ranging from 61% for 1 day curing to 88% for 7 and 28 days. In all cases, the final residual stain was below the visibility limit by the human eye.

Considering that applying the treatment after a short curing time (1 day) would be practically advantageous in the case of new buildings, as it would speed up the work, but also considering that applying the DPP solution after a longer curing time (7 or 28 days) leads to formation of a more continuous HAP coating, with the highest improvements in surface properties registered after 7 days, this latter duration of the cement hydration was selected as the most promising.

4. Conclusions

In the present study, we investigated the possibility of enhancing surface properties of hydrated Portland cement pastes by treating them with aqueous phosphate solutions to form *in situ* low-solubility, protective calcium phosphate coatings (CaP) on the surface. Based on the results, the following conclusions can be drawn.

1) *Precursor selection*. For all the investigated precursors (diammonium hydrogen phosphate - DAP, dipotassium hydrogen phosphate - DPP, and disodium hydrogen phosphate - DSP), surface CaP coatings were formed after 24 h of reaction at ambient conditions. Based on a combination of XRD and SEM-EDS, the CaP coating is thought to be mainly nanocrystalline hydroxyapatite (HAP). Thermodynamic modeling also predicted that these coatings would be composed of HAP, which is the most stable calcium phosphate phase at the reaction conditions. These CaP coatings were successful in improving surface resistance to abrasion, indentation and staining of the cementitious substrates. In the presence of DPP and DSP, some potassium and sodium were observed in the coatings; their amount decreased after prolonged immersion in water and drying, and in no case was any efflorescence observed visually. For all the precursors, the amount of soluble phosphates released into water where samples were immersed was found to be comparable to that of the untreated reference. Considering the superior performance exhibited by the

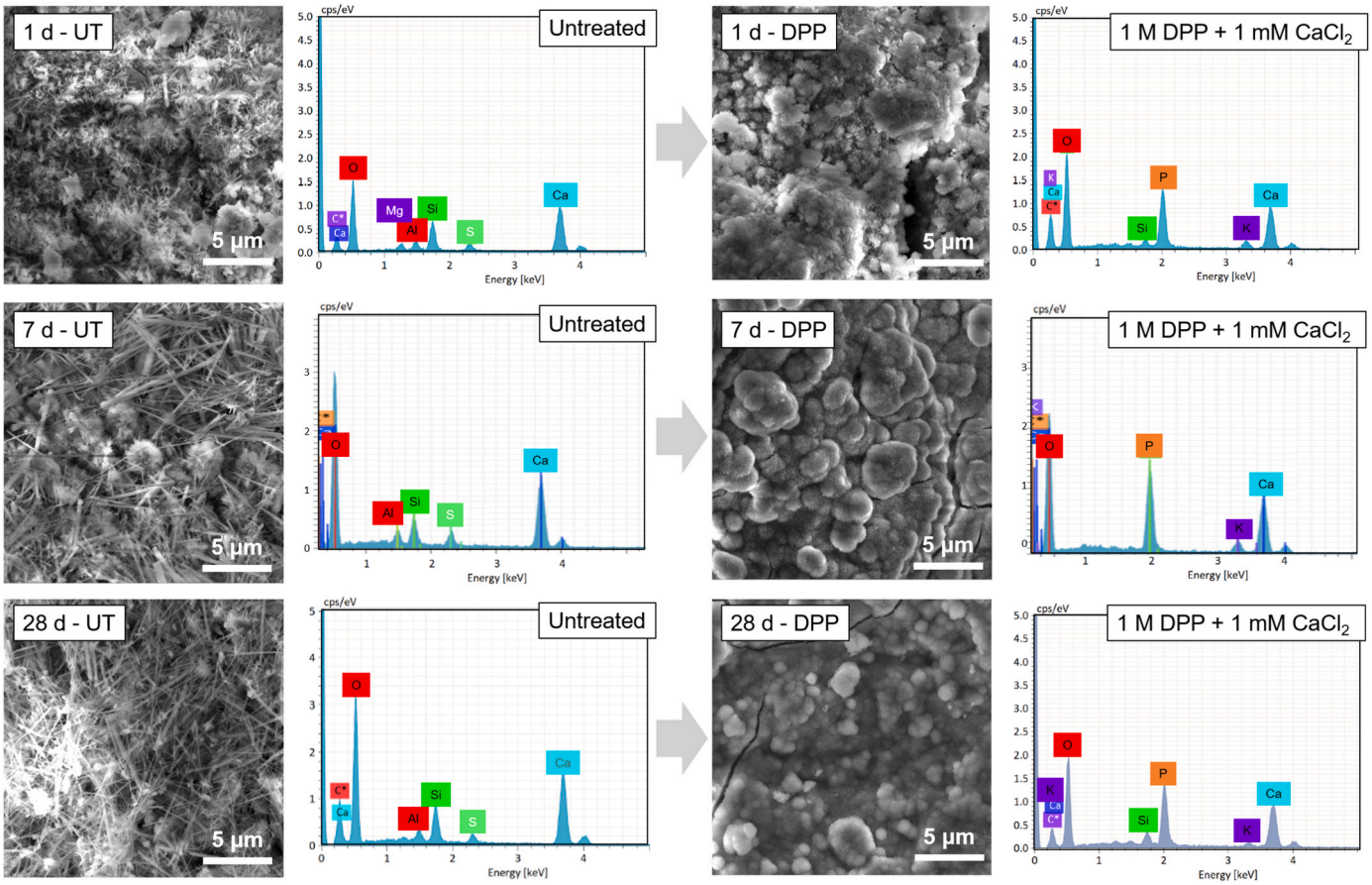

Fig. 14. SEM images and EDS spectra of the untreated references and samples treated with DPP at different curing times.

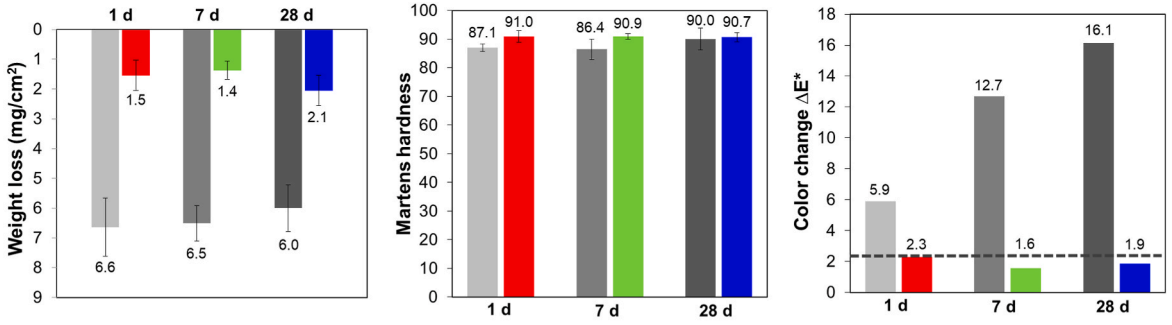

Fig. 15. Resistance to abrasion (left), indentation (center) and staining (right) of the untreated references (gray bars) and samples treated with DPP at different times (green bars). (For interpretation of the references to color in this figure legend, the reader is referred to the Web version of this article.)

DPP-treated samples, its behavior after water immersion, and the fact that it does not release NH_3 gas into the atmosphere (unlike DAP), DPP was selected as the most promising precursor.

2) *Selection of precursor concentration*. For the different DPP formulations compared (0.1 M, 1 M and 2 M, with addition of $CaCl_2$ in a 1:1000 M ratio to DPP), the 1 M DPP + 1 mM $CaCl_2$ formulation was found to provide the best combination: better surface property enhancement than the 0.1 M DPP + 0.1 mM $CaCl_2$ formulation, but without the formation of large potassium calcium phosphate hydrate ($KCaPO_4{\cdot}H_2O$) crystals like with the 2 M DPP + 2 mM $CaCl_2$ formulation. As $KCaPO_4{\cdot}H_2O$ is used as a fertilizer, it may be detrimental to the stability of the DPP-treated cement when exposed to water.
3) *Age of the cement when the treatment is applied*. In evaluating the effects of applying the selected formulation (1 M DPP + 1 mM $CaCl_2$) onto cement samples that were either 1, 7 or 28 days old, the optimum solution was found to be after 7 days of hydration, when formation of a continuous CaP coating and high surface mechanical improvement were registered, while the time gap between cement/mortar application and treatment administration for an applicator is also more reasonable, compared to after 28 days.

Overall, the present study highlighted that all three phosphate precursors, and especially dipotassium hydrogen phosphate (DPP), were promising candidates for the improvement of the surface properties of cementitious substrates. Because only a preliminary evaluation of treatment durability was performed in this study, future work should be dedicated to confirming that no undesired efflorescence is formed in the medium to long term and that the increase in mechanical performance is retained, even after repeated wetting-drying cycles. Future research

should be also dedicated to assessing the changes in permeability to liquids and gases, carbonation resistance and corrosion resistance after treatment.

Author contributions

Helene Pasco: Methodology; Software; Investigation; Writing - Original Draft; Visualization. Sonia Naidu: Conceptualization; Methodology; Investigation; Resources; Writing - Review & Editing; Project Administration; Funding acquisition. Barbara Lothenbach: Conceptualization; Methodology; Software; Writing - Review & Editing; Visualization; Funding acquisition. Enrico Sassoni: Conceptualization; Methodology; Resources; Writing - Review & Editing; Visualization; Supervision; Funding acquisition.

Declaration of competing interest

The authors declare that they have no known competing financial interests or personal relationships that could have appeared to influence the work reported in this paper. Sonia Naidu is an employee of Saint Gobain Research Paris, which provided funding for this research.

Data availability

The data that has been used is confidential.

Acknowledgements

Support from technicians at Saint-Gobain Research Paris (Anthony Train) and DICAM (Paolo Carta) and fruitful discussions with Dr. Nelly Brielles (Saint-Gobain Research Paris) and Dr. Frank Winnefeld (Empa) are gratefully acknowledged. Alessio Gabrielli (DICAM) is gratefully acknowledged for collaboration on ion chromatography.

References

[1] Z. Li, X. Zhou, H. Ma, D. Hou, Advanced Concrete Technology, John Wiley & Sons, 2022.
[2] European Standard 1504–2 (2004), Products and Systems for the Protection and Repair of Concrete Structures – Definitions, Requirements, Quality Control and Evaluation of Conformity. Part 2: Surface Protection Systems for Concrete, 2004.
[3] M. Safiuddin, Concrete damage in field conditions and protective sealer and coating systems, Coatings 7 (2017) 90, https://doi.org/10.3390/coatings7070090.
[4] E. Marie-Victoire, M. Bouichou, T. Congar, R. Blanchard, Concrete Cultural Heritage in France—inventory and State of Conservation, 2015.
[5] M. Delucchi, A. Barbucci, G. Cerisola, Study of the physico-chemical properties of organic coatings for concrete degradation control, Construct. Build. Mater. 11 (7) (1997) 365–371, https://doi.org/10.1016/S0950-0618(97)00060-3.
[6] A. Barbucci, M. Delucchi, G. Cerisola, Organic coatings for concrete protection: liquid water and water vapour permeabilities, Prog. Org. Coating 30 (4) (1997) 293–297, https://doi.org/10.1016/S0950-0618(97)00060-3.
[7] B. Pigino, A. Leemann, E. Franzoni, P. Lura, Ethyl silicate for surface treatment of concrete – Part II: characteristics and performance, Cement Concr. Compos. 34 (2012) 313–321, https://doi.org/10.1016/j.cemconcomp.2011. 11.021.
[8] G.W. Scherer, G.S. Wheeler, Silicate consolidants for stone, in: Key Engineering Materials, Trans Tech Publ, 2009, pp. 1–25.
[9] V. Daniele, G. Taglieri, L. Macera, G. Rosatelli, J. Otero, A.E. Charola, Green approach for an eco-compatible consolidation of the Agrigento biocalcarenites surface, Construct. Build. Mater. 186 (2018) 1188–1199, https://doi.org/10.1016/j.conbuildmat.2018.08.033.
[10] E. Franzoni, B. Pigino, C. Pistolesi, Ethyl silicate for surface protection of concrete: performance in comparison with other inorganic surface treatments, Cement Concr. Compos. 44 (2013) 69–76.
[11] E. Franzoni, H. Varum, M.E. Natali, M.C. Bignozzi, J. Melo, L. Rocha, E. Pereira, Improvement of historic reinforced concrete/mortars by impregnation and electrochemical methods, Cement Concr. Compos. 49 (2014) 50–58.
[12] I. Garcia-Lodeiro, R. Zarzuela, M.J. Mosquera, M.T. Blanco-Varela, Consolidation of artificial decayed portland cement mortars with an alkoxysilane-based impregnation treatment and its influence on mineralogy and pore structure, Construct. Build. Mater. 304 (2021), 124532.
[13] E. Sassoni, S. Naidu, G.W. Scherer, The use of hydroxyapatite as a new inorganic consolidant for damaged carbonate stones, J. Cult. Herit. 12 (2011) 346–355.
[14] S. Naidu, G.W. Scherer, Nucleation, growth and evolution of calcium phosphate films on calcite, J. Colloid Interface Sci. 435 (2014) 128–137.
[15] E. Sassoni, Hydroxyapatite and other calcium phosphates for the conservation of cultural heritage: a review, Materials 11 (2018) 557.
[16] J.-P. Lafon, E. Champion, D. Bernache-Assollant, Processing of AB-type carbonated hydroxyapatite Ca10- x (PO4) 6- x (CO3) x (OH) 2- x- 2y (CO3) y ceramics with controlled composition, J. Eur. Ceram. Soc. 28 (2008) 139–147.
[17] S.V. Dorozhkin, Calcium orthophosphates in nature, biology and medicine, Materials 2 (2009) 399–498.
[18] D.R. Lide, CRC Handbook of Chemistry and Physics, CRC press, 2004.
[19] S. Naidu, J. Blair, G.W. Scherer, Acid-resistant coatings on marble, J. Am. Ceram. Soc. 99 (2016) 3421–3428.
[20] G. Graziani, E. Sassoni, G.W. Scherer, E. Franzoni, Resistance to simulated rain of hydroxyapatite-and calcium oxalate-based coatings for protection of marble against corrosion, Corrosion Sci. 127 (2017) 168–174.
[21] G. Graziani, C. Colombo, C. Conti, E. Possenti, E. Perelli Cippo, M. Realini, E. Sassoni, Neutron radiography as a tool for assessing penetration depth and distribution of a phosphate consolidant for limestone, Construct. Build. Mater. 187 (2018) 238–247.
[22] E. Sassoni, E. Franzoni, Lime and cement mortar consolidation by ammonium phosphate, Construct. Build. Mater. 245 (2020), 118409.
[23] R.J. Turner, J.C. Renshaw, A. Hamilton, Biogenic hydroxyapatite: a new material for the preservation and restoration of the built environment, ACS Appl. Mater. Interfaces 9 (2017) 31401–31410.
[24] R.J. Turner, P. Bots, A. Richardson, P.A. Bingham, A. Scrimshire, A. Brown, M. S'Ari, J. Harrington, S.A. Cumberland, J.C. Renshaw, M.J. Baker, P.R. Edwards, C. Jenkins, A. Hamilton, (Hydroxy)apatite on Cement: Insights into a New Surface Treatment, 2021, pp. 6356–6368, https://doi.org/10.1039/d1ma00320h.
[25] D.A. Kulik, T. Wagner, S.V. Dmytrieva, G. Kosakowski, F.F. Hingerl, K. V. Chudnenko, U.R. Berner, GEM-Selektor geochemical modeling package: revised algorithm and GEMS3K numerical kernel for coupled simulation codes, Comput. Geosci. 17 (2013) 1–24.
[26] T. Thoenen, W. Hummel, U. Berner, E. Curti, The PSI/Nagra Chemical Thermodynamic Database, 12/07, 2014.
[27] B. Lothenbach, D.A. Kulik, T. Matschei, M. Balonis, L. Baquerizo, B. Dilnesa, G. D. Miron, R.J. Myers, Cemdata18: a chemical thermodynamic database for hydrated Portland cements and alkali-activated materials, Cement Concr. Res. 115 (2019) 472–506.
[28] B. Lothenbach, B. Xu, F. Winnefeld, Thermodynamic data for magnesium (potassium) phosphates, Appl. Geochem. 111 (2019), 104450.
[29] B. Xu, B. Lothenbach, F. Winnefeld, Influence of wollastonite on hydration and properties of magnesium potassium phosphate cements, Cement Concr. Res. 131 (2020), 106012.
[30] B. Xu, F. Winnefeld, B. Lothenbach, Effect of temperature curing on properties and hydration of wollastonite blended magnesium potassium phosphate cements, Cement Concr. Res. 142 (2021), 106370.
[31] B. Xu, F. Winnefeld, B. Ma, D. Rentsch, B. Lothenbach, Influence of aluminum sulfate on properties and hydration of magnesium potassium phosphate cements, Cement Concr. Res. 156 (2022), 106788.
[32] B. Xu, C. Cau Dit Coumes, D. Lambertin, B. Lothenbach, Compressive strength and hydrate assemblages of wollastonite-blended magnesium potassium phosphate cements exposed to different pH conditions, Cement Concr. Comp. (submitted for publication).
[33] E.C. Moreno, T.M. Gregory, W.E. Brown, Preparation and solubility of hydroxyapatite, J. Res. Nat. Bureau Standards. Sec. A, Phy. Chem. 72 (1968) 773.
[34] G. Ferraris, H. Fuess, W. Joswig, Neutron diffraction study of MgNH4PO4. 6H2O (struvite) and survey of water molecules donating short hydrogen bonds, Acta Crystallogr. Sect. B Struct. Sci. 42 (1986) 253–258.
[35] R.A. Robie, B.S. Hemingway, Thermodynamic Properties of Minerals and Related Substances at 298.15 K and 1 Bar (105 Pascals) Pressure and at Higher Temperatures, US Government Printing Office, 1995.
[36] H.C. Helgeson, Summary and critique of the thermodynamic properties of rock-forming minerals, Am. J. Sci. 278 (1978) 1–229.
[37] A.W. Frazier, J.P. Smith, J.R. Lehr, Precipitated Impurities of fertilizers prepared from wet-process phosphoric acid, J. Agric. Food Chem. 14 (1966) 522–529.
[38] H.F. McMurdie, M.C. Morris, E.H. Evans, B. Paretzkin, W. Wong-Ng, L. Ettlinger, C. R. Hubbard, Standard X-ray diffraction powder patterns from the JCPDS research associateship, Powder Diffr. 1 (1986) 64–77.
[39] W. Schwieger, H. Meyer zu Altenschildesche, G.T. Kokotailo, C.A. Fyfe, Low temperature syntheses of highly-ordered framework materials: the aluminium phosphate ammonium taranakite, Z. Anorg. Allg. Chem. 624 (1998) 1712–1717.
[40] J.J. Pluth, J.V. Smith, J.M. Bennett, J.P. Cohen, Structure of NH4Al2 (OH)(H2O) (PO4) 2. H2O, the ammonium–aluminum analog of GaPO4. 2H2O and leucophosphite, Acta Crystallogr. Sect. C Cryst. Struct. Commun. 40 (1984) 2008–2011.
[41] D. Louer, F. Deneuve, N. Ouillon, Powder diffraction data of potassium calcium phosphate KCa PO4. H2O, Powder Diffr. 2 (1987) 253–254.
[42] A.W. Fordham, U. Schwertmann, Composition and Reactions of Liquid Manure (Gülle), with Particular Reference to Phosphate: II. Solid Phase Components, Wiley Online Library, 1977.
[43] S. Lobanov, F. Koch, D. Mavinic, The Implication of Aqueous Equilibrium Modelling to Evaluate the Potential for Nutrient Recovery from Wastewater Streams, WEF/IWA Nutrient Removal and Recovery: Trends in Resource Recovery and Use, Vancouver, BC, Canada, USB Proceedings), 2013.
[44] A.P. Bayuseno, W.W. Schmahl, Thermal decomposition of struvite in water: qualitative and quantitative mineralogy analysis, Environ. Technol. 41 (2020) 3591–3597.

[45] A.W. Taylor, A.W. Frazier, E.L. Gurney, Solubility products of magnesium ammonium and magnesium potassium phosphates, Trans. Faraday Soc. 59 (1963) 1580–1584.
[46] A.W. Taylor, A.W. Frazier, E.L. Gurney, J.P. Smith, Solubility products of di- and tri-magnesium phosphates and the dissociation of magnesium phosphate solutions, Trans. Faraday Soc. 59 (1963) 1585–1589.
[47] J.R. Burns, B. Finlayson, Solubility product of magnesium ammonium phosphate hexahydrate at various temperatures, J. Urol. 128 (1982) 426–428.
[48] K.N. Ohlinger, T.M. Young, E.D. Schroeder, Predicting struvite formation in digestion, Water Res. 32 (1998) 3607–3614.
[49] S. Lobanov, Personal Communication 14, 8, 2018, 2018.
[50] V. Babić-Ivančić, J. Kontrec, D. Kralj, L. Brečević, Precipitation diagrams of struvite and dissolution kinetics of different struvite morphologies, Croat. Chem. Acta 75 (2002) 89–106.
[51] V. Babić-Ivančić, J. Kontrec, L. Brečević, D. Kralj, Kinetics of struvite to newberyite transformation in the precipitation system MgCl2–NH4H2PO4–NaOH–H2O, Water Res. 40 (2006) 3447–3455.
[52] M.I.H. Bhuiyan, D.S. Mavinic, R.D. Beckie, A solubility and thermodynamic study of struvite, Environ. Technol. 28 (2007) 1015–1026.
[53] M. Hanhoun, L. Montastruc, C. Azzaro-Pantel, B. Biscans, M. Frèche, L. Pibouleau, Temperature impact assessment on struvite solubility product: a thermodynamic modeling approach, Chem. Eng. J. 167 (2011) 50–58.
[54] A.W. Taylor, E.L. Gurney, Solubilities of potassium and ammonium taranakites, J. Phys. Chem. 65 (1961) 1613–1616.
[55] A.W. Taylor, E.L. Gurney, The dissolution of basic potassium and ammonium aluminum phosphates, Soil Sci. Soc. Am. J. 28 (1964) 289–290.
[56] A.W. Taylor, E.L. Gurney, Precipitation of phosphate by iron oxide and aluminum hydroxide from solutions containing calcium and potassium, Soil Sci. Soc. Am. J. 29 (1965) 18–22.
[57] B. Xu, F. Winnefeld, J. Kaufmann, B. Lothenbach, Influence of magnesium-to-phosphate ratio and water-to-cement ratio on hydration and properties of magnesium potassium phosphate cements, Cement Concr. Res. 123 (2019), 105781.
[58] B. Lothenbach, B. Bary, P. Le Bescop, T. Schmidt, N. Leterrier, Sulfate ingress in Portland cement, Cement Concr. Res. 40 (2010) 1211–1225.
[59] G. Graziani, E. Sassoni, E. Franzoni, G.W. Scherer, Hydroxyapatite coatings for marble protection: optimization of calcite covering and acid resistance, Appl. Surf. Sci. 368 (2016) 241–257.
[60] E. Sassoni, G. Graziani, E. Franzoni, G.W. Scherer, Calcium phosphate coatings for marble conservation: influence of ethanol and isopropanol addition to the precipitation medium on the coating microstructure and performance, Corrosion Sci. 136 (2018) 255–267.
[61] F. Winnefeld, A. Schöler, B. Lothenbach, Sample preparation, in: K.L. Scrivener, R. Snellings, B. Lothenbach (Eds.), A Practical Guide to Microstructural Analysis of Cementitious Materials, CRC Press, Boca Raton, FL, USA, 2016, 2016.
[62] F. Sandrolini, E. Franzoni, G. Cuppini, Predictive diagnostics for decayed ashlars substitution in architectural restoration in Malta, Mater. Eng. Modena. 11 (2000) 323–338.
[63] European Standard 15801, Conservation of Cultural Property - Test Methods - Determination of Water Absorption by Capillarity, 2010.
[64] S.V. Dorozhkin, Calcium orthophosphates: occurrence, properties, biomineralization, pathological calcification and biomimetic applications, Biomatter 1 (2011) 121–164, https://doi.org/10.4161/biom.18790.
[65] A. Garley, S.E. Hoff, N. Saikia, S. Jamadagni, A. Baig, H. Heinz, Adsorption and substitution of metal ions on hydroxyapatite as a function of crystal facet and electrolyte pH, J. Phys. Chem. C 123 (2019) 16982–16993.
[66] A. Ressler, A. Žužić, I. Ivanišević, N. Kamboj, H. Ivanković, Ionic substituted hydroxyapatite for bone regeneration applications: a review, Open Ceramics 6 (2021), 100122.
[67] J. Sang Cho, S.-H. Um, D. Su Yoo, Y.-C. Chung, S. Hye Chung, J.-C. Lee, S.-H. Rhee, Enhanced osteoconductivity of sodium-substituted hydroxyapatite by system instability, J. Biomed. Mater. Res. B Appl. Biomater. 102 (2014) 1046–1062.
[68] E. Boanini, M. Gazzano, A. Bigi, Ionic substitutions in calcium phosphates synthesized at low temperature, Acta Biomater. 6 (6) (2010) 1882–1894, https://doi.org/10.1016/j.actbio.2009.12.041.
[69] R.D. Shannon, Revised effective ionic radii and systematic studies of interatomic distances in halides and chalcogenides, Acta Crystallogr. Sect. A Cryst. Phys. Diffr. Theor. Gen. Crystallogr. 32 (1976) 751–767.
[70] G. Sharma, Color fundamentals for digital imaging, in: Digital Color Imaging Handbook, CRC press, 2017, pp. 1–114.
[71] A.G. Evans, M.D. Drory, M.S. Hu, The cracking and decohesion of thin films, J. Mater. Res. 3 (1988) 1043–1049.
[72] E.C. Moreno, R. T Zahradnik, A. Glazman, R. Hwu, Precipitation of hydroxyapatite from dilute solutions upon seeding, Calcif. Tissue Res. 24 (1977) 47–57.
[73] K. Scrivener, V.M. John, E.M. Gartner, Eco-efficient cements: potential economically viable solutions for a low-CO_2 cement-based materials industry, Cement Concr. Res. 114 (2018) 2–26, https://doi.org/10.1016/j.cemconres.2018.03.015.